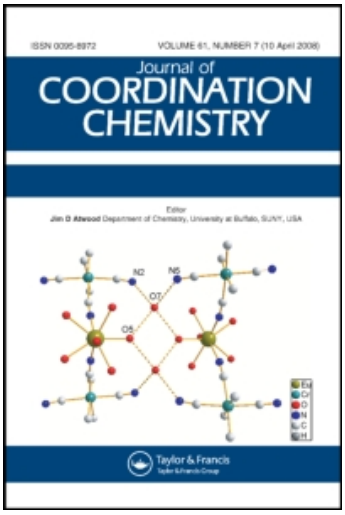

Journal of Coordination Chemistry
Publication details, including instructions for authors and subscription information:
http://www.informaworld.com/smpp/title~content=t713455674

Uranyl and transition metal chelates of tenoxicam. Crystal structures of trans,trans-[Co(II)(Hten)$_2$(dmso)$_2$], trans,trans-[Zn(II)(Hten)$_2$(dmso)$_2$] and cis,cis-[UO$_2$(VI)(Hten)$_2$(H$_2$O)] · 2C$_2$H$_5$OH

Nadia E. A. El-Gamel[a]; Daniela Gerlach[b]
[a] Chemistry Department, Faculty of Science, 12613 Giza, Egypt [b] Institut für Anorganische Chemie, 09596 Freiberg, Germany

To cite this Article El-Gamel, Nadia E. A. and Gerlach, Daniela(2008) 'Uranyl and transition metal chelates of tenoxicam. Crystal structures of **trans,trans**-[Co(II)(Hten)$_2$(dmso)$_2$], **trans,trans**-[Zn(II)(Hten)$_2$(dmso)$_2$] and **cis,cis**-[UO$_2$(VI)(Hten)$_2$(H$_2$O)] · 2C$_2$H$_5$OH', Journal of Coordination Chemistry, 61: 14, 2246 — 2265
To link to this Article: DOI: 10.1080/00958970801904786
URL: http://dx.doi.org/10.1080/00958970801904786

Journal of Coordination Chemistry
Vol. 61, No. 14, 20 July 2008, 2246–2265

Uranyl and transition metal chelates of tenoxicam. Crystal structures of *trans*,*trans*-[Co(II)(Hten)$_2$(dmso)$_2$], *trans*,*trans*-[Zn(II)(Hten)$_2$(dmso)$_2$] and *cis*,*cis*-[UO$_2$(VI)(Hten)$_2$(H$_2$O)]·2C$_2$H$_5$OH

NADIA E. A. EL-GAMEL*† and DANIELA GERLACH‡

†Chemistry Department, Faculty of Science, Cairo University, 12613 Giza, Egypt
‡Institut für Anorganische Chemie, TU Bergakademie, Leipziger Strasse 29, 09596 Freiberg, Germany

(*Received 29 March 2007; in final form 21 September 2007*)

The synthesis and characterization of ternary Fe(III)- (**1**), Co(II)- (**2**), Ni(II)- (**3**), Cu(II)- (**4**), Zn(II)- (**5**) and UO$_2$(VI)- (**6**) chelates with the potent anti-inflammatory drug tenoxicam (H$_2$ten) and (dl-alanine, Hala) are reported. All complexes are octahedral except Cu(II) and Zn(II) chelates, which are tetrahedral, and U-atoms in the uranyl chelates have a pentagonal-bipyramidal coordination sphere. The ternary Co(II) and Zn(II) complexes dissociate in dmso where orange and yellow crystals of *trans*,*trans*-[Co(II)(Hten)$_2$(dmso)$_2$] (**8**) and *trans*,*trans*-[Zn(II)(Hten)$_2$(dmso)$_2$] (**9**), respectively, were obtained. Crystallization of the binary uranyl chelate (**7**) from ethanol afforded the ethanol solvate *cis*,*cis*-[UO$_2$(VI)(Hten)$_2$(H$_2$O)]·2C$_2$H$_5$OH (**7a**). *trans*,*trans*-[Co(II)(Hten)$_2$(dmso)$_2$] (**8**) and *trans*,*trans*-[Zn(II)(Hten)$_2$(dmso)$_2$] (**9**) crystallize in the monoclinic space group $P2_1/n$ while **7a** crystallizes in the triclinic space group $P\bar{1}$. The kinetics of the thermal decompositions for **1**, **3**, **4**, **6** and **7** were studied and the thermodynamic parameters E*, ΔH*, ΔS* and ΔG* evaluated.

Keywords: Tenoxicam; dl-alanine; Metal chelates; Vibrational spectra; Thermal behavior; X-ray crystal structure

1. Introduction

Metal complexes containing non-steroidal anti-inflammatory drugs (NSAIDs) from the oxicam family have gained much attention and increasing interest for inorganic, pharmaceutical and medicinal chemistry as an approach to drug development [1, 2], showing promise against inflammatory and rheumatic diseases [3]. Oxicams are the most important members of NSAIDs, as they have several potential donors to metal ions. Manifold arrangements of metal and ligand can be obtained [4].

Piroxicam (H$_2$pir), meloxicam (H$_2$mel) and tenoxicam (H$_2$ten) (figure 1) are the most important members of the oxicam class, due to their potential activity in biomedical chemistry and as strong chelators for several divalent metal ions. In particular, tenoxicam (H$_2$ten) is considered as the clinically most often used and most studied

*Corresponding author. Email: nadinealy@hotmail.com

ISSN 0095-8972 print/ISSN 1029-0389 online © 2008 Taylor & Francis
DOI: 10.1080/00958970801904786

species of the oxicam family. It differs from piroxicam in having a thiophene ring in place of benzene, which may enhance the clinical activity of the drug [5]. Piroxicam (H_2pir) exhibits three different coordination modes towards metal ions as shown by X-ray diffraction experiments [6, 7]. H_2pir reacted as a singly deprotonated chelating ligand via pyridyl nitrogen and amide oxygen towards Cu(II) and Cd(II) [7a], as a monodentate ligand via pyridyl nitrogen towards Pt(II) [7b,c] and as a dianionic tridentate ligand via amide oxygen and nitrogen, and pyridyl nitrogen towards Sn(IV) [6].

Depending on the polarity of the solvent, the extended electron conjugation over H_2ten can give rise to zwitterions [8] making the acidity of the enolic group remarkably higher [9] due to the weak basicity of pyridinyl group, as shown in figure 1. The acid–base behavior of H_2ten was also studied and its corresponding pK_a values have been reported [9, 10].

Tenoxicam itself has been investigated using various analytic methods [8, 11–16]. It forms complexes with first row transition metal ions, including Fe(III), Co(II), Ni(II), Cu(II) and Mn(II); spectroscopic and magnetic properties suggest that H_2ten is a monoanionic ligand through the enolate and amide oxygen atoms [17]. However, single crystal structure analysis of $[Cu(Hten)_2(py)_2] \cdot EtOH$ and $[Cd(Hten)_2(dmso)_2]$ revealed that H_2ten formed stable chelates by employing the amide oxygen and pyridyl nitrogen

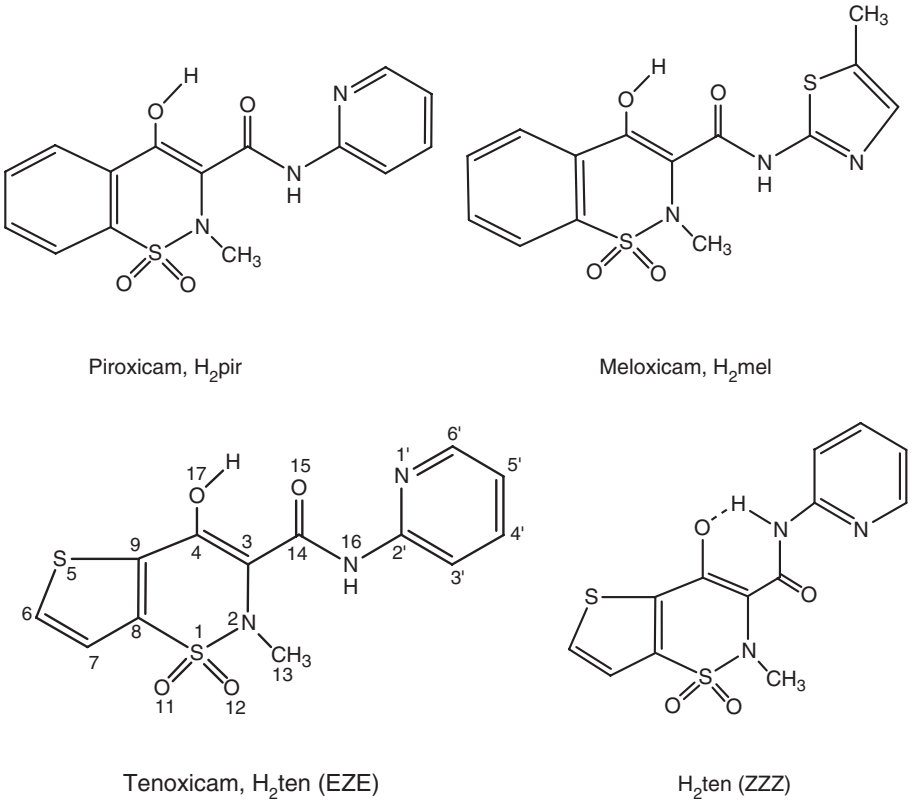

Figure 1. Structural formula of piroxicam (H_2pir), meloxicam (H_2mel) and tenoxicam (H_2ten) with demonstration of EZE and ZZZ conformations.

in these cases [11, 18]. In addition, complex formation between H_2ten (and H_2pir) with alkaline earth cations have been reported [11]. Differential pulse polarography and cyclic voltammetry experiments with Cu(II), Pb(II) and Cd(II) complexes of H_2ten and H_2pir have been done [19]; H_2ten exhibited stronger chelating properties than H_2pir towards each ion despite their structural similarity. Other authors [20] have investigated the interaction of H_2ten with Fe(III), Sb(III), Bi(III), Cr(II), Cd(II) and Al(III) using potentiometric and fluorimetric methods as well as the fluorescence properties of the drug in absence and presence of metal ions.

Organotin(IV) complexes with H_2ten and H_2pir have attracted much attention due to potential of tin-based antitumor drugs, and spectral characterization and investigation of organotin complexes of both drugs are reported [21].

Complex formation of H_2ten with Zn(II) and Cu(II) enhanced tenoxicam activity [22], therefore, many authors have studied the complex formation with β- or γ-cyclodextrin in order to improve the aqueous solubility of the drug and to decrease its side effects [23].

Very recently Zayed *et al.* [24] reported synthesis and thermal characterization of ternary chelates of some d-block metal ions with H_2ten and phenylalanine and glycine, respectively. In the present work the synthesis and characterization of uranyl and transition metal complexes of H_2ten with dl-alanine have been performed to further explore this class of complexes. The structures of the complexes were elucidated using elemental analysis, IR, Raman, magnetic susceptibility, solid reflectance and thermogravimetric analysis. Additionally, a solvate uranyl binary chelate is synthesized and characterized by single crystal X-ray diffraction. Co(II) and Zn(II) ternary chelates showed dissociation in hot dmso solution and single crystals of *trans*,*trans*-[Co(II)(Hten)$_2$(dmso)$_2$] (**8**) and *trans*,*trans*-[Zn(II)(Hten)$_2$(dmso)$_2$] (**9**) were obtained.

2. Experimental

2.1. *Reagents*

All chemicals used were of analytical reagent grade (AR): tenoxicam (sample was supplied by Eipico company, Egypt, and its melting point was checked to confirm its purity (210°C)), dl-alanine (Sigma), cobalt(II) and nickel(II) chlorides hexahydrated (BDH), zinc and copper acetate dehydrated (Ubichem), ferric chloride hexahydrated (Prolabo), uranyl nitrate (Sigma), ethanol and dimethylformamide (Merck). All solutions were prepared with de-ionized water.

2.2. *Synthesis of the chelates*

Metal complexes were synthesized by addition of a hot water-ethanolic solution (60°C) of the metal chlorides for Fe(III), Co(II) and Ni(II), nitrate for UO_2(VI) or acetate for Cu(II) and Zn(II) (25 mL, 0.1 mmol) to a hot ethanolic solution of both H_2ten (25 mL, 0.2 mmol in case of binary or 0.1 mmol in case of ternary complexes) and dl-alanine (0.1 mmol). The resulting mixture was stirred under reflux for 2 h and left to cool, whereby the complexes precipitated as fine powders. The solid complexes were filtered, washed with ethanol, then with diethyl ether, and dried in a vacuum desiccator over

anhydrous calcium chloride. Orange single crystals of *cis*,*cis*-$[UO_2(VI)(Hten)_2(H_2O)] \cdot 2C_2H_5OH$ (**7a**) suitable for X-ray analysis were obtained by recrystallization from ethanol. $[Co(H_2ten)(ala)Cl(H_2O)] \cdot 2H_2O$ (**2**) and $Zn(H_2ten)(ala)](AcO) \cdot 3H_2O$ (**5**) chelates show some dissociation in dmso solution, where orange and yellow single crystals suitable for X-ray analysis of *trans*,*trans*-$[Co(II)(Hten)_2(dmso)_2]$ (**8**) and *trans*,*trans*-$[Zn(II)(Hten)_2(dmso)_2]$ (**9**) were grown upon slow evaporation at room temperature for several days (table 2, represents analytical and physical data of metal chelates).

2.3. *Physical measurements*

All chemicals were of the highest purity available. Elemental analyses (C, H, N, S) were performed in the Microanalytical Center at Cairo University. FTIR spectra were recorded at room temperature using a 1430 Perkin-Elmer FT-IR spectrometer. The samples were thoroughly mixed with dried KBr. The spectra were collected from 400–4000 cm^{-1}. Raman spectra were recorded on a Bruker RFS 100/S module with a Nd:YAG laser ($\lambda = 1064$ nm) in the backscattering (180°) configuration. The focused laser beam diameter was about 10 μm and the spectral resolution was 4 cm^{-1}. NMR spectra were recorded on a BRUKER DPX 400 instrument at room temperature (d_6-DMSO solution with TMS as internal standard). Thermal analyses of the complexes were carried out using a Shimadzu TGA-50H and DTA-50H thermogravimetric analyzer in a dynamic nitrogen atmosphere (flow rate 20 mL min^{-1}) with a heating rate of 10°C min^{-1}. The percentage weight loss was measured from ambient temperature to 1000°C. Highly sintered α-Al_2O_3 was used as reference. The molar conductance measurements of the complexes were carried out in DMF using a Genway 4200 conductivity meter. The molar magnetic susceptibilities of the powdered samples were measured by the Faraday method (magnetic susceptibility balance—Sherwood were made by Pascal's constant using $Hg[Co(SCN)_4]$ as calibrant). The diffuse reflectance spectra were recorded using a Shimadzu 3101pc spectrophotometer; the spectra were recorded as $BaSO_4$ disks. Metal content of the complexes were determined by titration against standard EDTA after complete decomposition of the complexes with aqua regia in 50 mL digestion flasks.

2.4. *Crystallographic structure determination*

Single crystal X-ray data were recorded on a BRUKER-NONIUS-X8 APEXII-CCD-diffractometer with Mo-Kα radiation ($\lambda = 0.71073$ Å). The structures were solved with direct methods and refined with full-matrix least squares methods; all non-hydrogen atoms were anisotropically refined. All C-bonded hydrogen atoms (in case of **7a** all hydrogen atoms) were placed in idealized positions (riding model) and isotropically refined. Amide hydrogen atoms of **8** and **9** were detected by analysis of the residual electron density and isotropically refined without restraints. Structure solution and refinement of F^2 against all reflections were performed with SHELXS-97 and SHELXL-97 (G.M. Sheldrick, Universität Göttingen, 1986–1997). The structure of **6** bears two ethanol molecules in the asymmetric unit. Each is twofold disordered by means of cross-wise disordered $–CH_2–CH_3$ groups and non-crossing C–O bonds. The (initially isotropic and then anisotropic) thermal displacement parameters of the

ethanol C– and O–atoms were restrained to be equal for atoms in corresponding positions, C–C distances were restrained to be equal within one molecule (fixed to 1.54 Å in one of them) and the C–O distances were also restrained to the same length (fixed to 1.40 Å in one of the molecules) and the site occupancies were refined. The final refinement (anisotropic C– and O–atoms, H-atoms in idealized positions, riding model) was carried out with fixed site occupancies (s.o.f. 0.76: 0.24 and 0.69: 0.31). Crystallographic data and the details of data collection are listed in table 1.

3. Results and discussion

Table 2 gives the results of the elemental analyses (C, H, N, S and metal content) with the proposed molecular formula. The metal content values are average values of the metal contents determined by titration and those deduced from the metallic residues. The results obtained are in good agreement with those calculated for the suggested formula. The molar conductance values of the solid complexes (Λ_m, $\Omega^2\,cm^{-1}\,mol^{-1}$) were measured. The ligands form 1 : 1 : 1 (M:H_2ten:ala) complexes where Hala coordinates to the metal ions via deprotonated carboxylate (ala^- form) and amino N-atom. The solids were isolated in the general formula

Table 1. Crystallographic data and structure refinement for *cis,cis*-$[UO_2(VI)(Hten)_2(H_2O)]\cdot 2C_2H_5OH$ (**7a**), *trans,trans*-$[Co(II)(Hten)_2(dmso)_2]$ (**8**) and *trans,trans*-$[Zn(II)(Hten)_2(dmso)_2]$ (**9**).

	7a	**8**	**9**
Formula	$C_{30}H_{34}N_6O_{13}S_4U$	$C_{30}H_{32}CoN_6O_{10}S_6$	$C_{30}H_{32}N_6O_{10}S_6Zn$
M_r	1052.90	887.91	394.35
Cryst. syst.	Triclinic	Monoclinic	Monoclinic
Cryst. color	Orange	Orange	Yellow
Space group	$P\bar{1}$	$P2_1/n$	$P2_1/n$
a (Å)	9.6062(3)	7.6144(2)	7.6515(2)
b (Å)	13.0886(4)	13.9792(4)	13.9775(4)
c (Å)	16.3728(5)	16.9627(4)	16.9422(5)
α (°)	101.167(2)	90	90
β (°)	101.439(2)	95.943(1)	95.885(2)
γ (°)	91.806(2)	90	90
V (Å^3)	1974.25(11)	1795.86(8)	1802.40(9)
Z	2	2	2
ρ_{calcd} ($g\,cm^{-3}$)	1.771	1.642	1.648
μ(Mo-Kα) (mm^{-1})	4.390	0.892	1.094
T (K)	90(2)	90(2)	90(2)
Cryst. dimens. (mm^3)	$0.41 \times 0.20 \times 0.08$	$0.36 \times 0.32 \times 0.17$	$0.29 \times 0.26 \times 0.13$
θ_{max} (°)	38.5	45.0	40.0
F(000)	1032	914	920
Reflns. collected	82897	73397	56319
Indep. reflns.	22054 ($R_{int} = 0.0390$)	14748 ($R_{int} = 0.0482$)	10993 ($R_{int} = 0.0563$)
R_1[a] [$I > 2\sigma(I)$]	0.0399	0.0368	0.0378
wR_2[b] [$I > 2\sigma(I)$]	0.0851	0.0926	0.0873
R_1 (all data)	0.0661	0.0602	0.0666
wR_2 (all data)	0.0912	0.0997	0.0994
Largest diff. peak, hole ($e\,Å^{-3}$)	2.876, −1.184	0.709, −0.888	0.720, −0.738

[a] $R_1 = \sum\|F_o| - |F_c\|/\sum|F_c|$.
[b] $wR_2 = [\sum w(F_o^2 - F_c^2)^2/\sum w(F_o^2)^2]^{1/2}$.

Table 2. Analytical and physical data of metal chelates.

Compound	Color (% yield)	m.p. (°C)	Found (calculated) %					μ_{eff} (B.M.)	Λ_m ($\Omega^2 mol^{-1} cm^{-1}$)
			C	H	N	S	M		
Tenoxicam (H_2ten)	Yellow	210	46.35	3.55	12.20	19.25	–	–	–
$C_{13}H_{11}N_3O_4S_2$			(46.28)	(3.29)	(12.46)	(18.97)			
$[Fe(III)(H_2ten)(ala)Cl_2]\cdot 2H_2O$	Brown	>300	32.50	3.45	9.43	10.68	9.09	6.55	11.96
$C_{16}H_{21}Cl_2FeN_4O_8S_2$	(73)		(32.67)	(3.57)	(9.52)	(10.88)	(9.49)		
$[Co(II)(H_2ten)(ala)Cl(H_2O)]\cdot 2H_2O$	Yellow	>300	33.16	3.92	10.03	11.43	9.83	5.32	17.16
$C_{16}H_{23}ClCoN_4O_9S_2$	(85)		(33.48)	(4.01)	(9.76)	(11.16)	(10.27)		
$[Ni(II)(H_2ten)(ala)Cl(H_2O)]\cdot 3H_2O$	Olive green	>300	32.41	4.22	9.63	10.58	10.15	3.65	10.99
$C_{16}H_{25}ClN_4NiO_{10}S_2$	(79)		(32.48)	(4.30)	(9.47)	(10.83)	(9.93)		
$[Cu(II)(H_2ten)(ala)](AcO)$	Yellowish green	>300	39.34	3.59	10.05	11.38	11.12	2.02	63.95
$C_{18}H_{20}CuN_4O_8S_2$	(82)		(39.45)	(3.65)	(10.22)	(11.70)	(11.60)		
$[Zn(II)(H_2ten)(ala)](AcO)\cdot 3H_2O$	Yellow	>300	36.00	4.10	9.42	10.35	10.52	Diamagnetic	78.96
$C_{18}H_{26}N_4O_{11}S_2Zn$	(85)		(35.82)	(4.31)	(9.29)	(10.61)	(10.78)		
$[UO_2(VI)(Hten)(ala)(H_2O)]$	Orange	>300	28.35	2.55	8.69	9.47	–	Diamagnetic	12.88
$C_{16}H_{18}N_4O_9S_2U$	(69)		(26.96)	(2.52)	(7.86)	(8.98)	–		
$[UO_2(VI](Hten)_2(H_2O)]$	Orange	>300	33.50	2.20	9.02	13.25	–	Diamagnetic	13.34
$C_{26}H_{22}N_6O_{11}S_4U$	(62)		(33.50)	(2.29)	(8.75)	(13.33)	–		

$[M(H_2ten)(ala)(Cl)_n(H_2O)_m]\cdot yH_2O$ (M=Fe(III) ($n=2$, $m=0$, $y=2$), Co(II) ($n=1$, $m=1$, $y=2$) and Ni(II) ($n=1$, $m=1$, $y=3$); $[M(H_2ten)(ala)](X)_z\cdot yH_2O$ (M=Cu(II) (X = AcO, $z=1$, $y=0$), Zn(II) (X = AcO, $z=1$, $y=3$) and $[UO_2(VI)(Hten)_x(Y)(H_2O)]$ (for binary chelate $x=2$, Y = 0; for ternary chelate $x=1$, Y = ala)).

3.1. *Vibrational spectra*

The free H_2ten ligand shows a strong band at 1636 cm^{-1} characteristic of a carbonyl stretching vibration of the secondary amide group (–CO–NH–). Shifts in this band to lower (2–37 cm^{-1}) or to higher frequencies (3–4 cm^{-1}) indicate its involvement in chelate formation [24–26]. In Raman spectra this band is shifted from 1606 cm^{-1} to lower frequencies (8–24 cm^{-1}) in the complexes.

The band at 1599 cm^{-1} is assigned to the ν(C=N) stretching vibration of the pyridyl moiety. Coordination of the pyridyl nitrogen is indicated by a 14–29 cm^{-1} shift to lower wavenumbers or 7–14 cm^{-1} shift to higher wavenumbers [27–29], in addition its participation is confirmed from the band due to in-plane deformation ρ(py) at 624 cm^{-1}. After complexation, this band disappears and a new band at 637–644 cm^{-1} is found [30].

In uranyl chelates two intense sharp bands (916, 918 cm^{-1}); (773, 774 cm^{-1}) were reliably assigned to asymmetric and symmetric stretching vibrations of O=U=O in binary and ternary chelates, respectively [31]; these two bands were observed at 990 and 835 cm^{-1} in Raman spectra [32].

IR spectra of Hala show sharp bands at 1586 and 1412 cm^{-1} assigned to the asymmetric and symmetric stretching vibrations of the carboxylate moiety, respectively. These bands are shifted to lower (3–63 cm^{-1}) or higher (12–22 cm^{-1}) frequencies, while in Raman spectra these bands appear in the 1597–1575 cm^{-1} and 1383–1310 cm^{-1} region indicating that Hala coordinates to the metal ions via deprotonated carboxylate [26].

Overlap between water of hydration and/or coordination with the NH_2 characteristic vibration band at 3300–3200 cm^{-1} prevents determining chelation, therefore, we focused on in-plane bending, $\delta(NH_2)$ vibration; the shift of this band from 1502 cm^{-1} to 1462–1527 cm^{-1} indicates participation in complex formation [24, 29].

New bands in the complexes at 586–523 and 536–514 cm^{-1} can be assigned to the ν(M–O) stretching vibrations of the carbonyl and carboxylate groups, respectively [24, 29]. Bands in the 497–476 cm^{-1} and 432–417 cm^{-1} regions are attributed to the ν(M–N) stretching vibration of the pyridyl and amino groups [24, 29].

Raman spectra showed new bands in the range 430–474 and 341–334 cm^{-1} which are assigned to the M–O and M–N stretching vibrations, respectively [33, 34]; further weak bands found at 698 and 699 cm^{-1} in uranyl chelates are assigned to the U–O vibrations of coordinated water [35].

3.2. *Molar conductivity measurements*

As seen from table 2, the molar conductivity values for **1**, **2**, **3**, **6** and **7** were in the range 17.16–10.99 $\Omega^2\,cm^{-1}\,mol^{-1}$. These relatively low values indicate non-electrolytic nature of these chelates [36, 37]. The molar conductance values (table 2) for **4** and **5** were found

Table 3. Assignment of the IR spectra for **1**–**7**.

Compound	ν(CO–NH)	ν(C=N)	ρ(py)	$\nu(SO_2)$ (asym)	$\nu(SO_2)$ (sym)	ν(COO) (asym)	ν(COO) (sym)	$\delta(NH_2)$	ν(M–O)	ν(M–O)	ν(M–N)	ν(M–N)
H_2ten	1636s	1599s	624s	1330s	1041s	–	–	–	–	–	–	–
Hala	–	–	–	–	–	1586s	1412s	1502s	–	–	–	–
1	1599m	1570m	637s	1351s	1042m	1526s	1431s	1462m	568m	524m	486m	417w
2	1640m	1606m	644s	1330s	1042s	1582s	1427s	1522s	584m	536m	497w	417w
3	1639w	1585w	640m	1330s	1044s	1525m	1424m	1487m	586m	536m	472m	432m
4	1632w	1606s	643s	1333s	1042s	1577s	1424m	1516s	546m	514m	476w	420w
5	1634w	1613w	640s	1330s	1046s	1583s	1424s	1527s	586m	536m	480w	428w
6	1600s	–	–	1344m	1041s	1523s	1434s	1464s	566m	522m	–-	430w
7	1600s	–	–	1342m	1042s	–	–	–	523m	–	–-	–

s = strong, m = medium, w = weak.

to be 63.95 and 78.96 $\Omega^2\,cm^{-1}\,mol^{-1}$, respectively. The relatively high values indicate 1 : 1 electrolytes [37, 38].

3.3. *Magnetic susceptibility measurements*

The magnetic moment values are calculated and reported in table 2. $[Fe(III)(H_2ten)(ala)Cl_2]\cdot 2H_2O$ (**1**) has a μ_{eff} value of 6.55 B.M., indicating a high spin octahedral geometry [29, 39]. $[Co(II)(H_2ten)(ala)Cl(H_2O)]\cdot 2H_2O$ (**2**) and $[Ni(II)(H_2ten)(ala)Cl(H_2O)]\cdot 3H_2O$ (**3**) have a magnetic momentum of 5.32 and 3.65 B.M., respectively, also indicating a high spin octahedral configuration [24, 40, 41]. [Cu(II)(H_2ten)(ala)](AcO) (**4**) has $\mu_{eff} = 2.02$ B.M., indicating a tetrahedral geometry for this complex [41]. UO_2(VI) and Zn(II) chelates are diamagnetic.

3.4. *Diffuse reflectance measurements*

From the diffuse reflectance spectrum, **1** exhibits a band at 20,704 cm^{-1}, which may be assigned to the $^6A_{1g} \rightarrow {}^6T_2g$ (G) transition in octahedral geometry of the complex [42]. The $^6A_{1g} \rightarrow {}^6T_1g$ transition appears to be split into two bands at 12,121 cm^{-1} and 18,298 cm^{-1}. A medium broad absorption band in the area from 33,333 cm^{-1} to 24,390 cm^{-1} could be related to LMCT [43].

For **2**, the reflectance spectrum shows three bands at 13,333, 15,748 and 21,053 cm^{-1} which are assigned to $^4T_{1g}$ (F) $\rightarrow {}^4T_{2g}$ (F), $^4T_{1g}$ (F) $\rightarrow {}^4E_{2g}$ (F) and $^4T_{1g}$ (F) $\rightarrow {}^4T_{2g}$ (P) transitions, respectively, consistent with octahedral geometry for Co(II) complex. The band at 25,316 cm^{-1} is LMCT [40].

The electronic spectrum of **3** displays three bands which are assigned as follows: 12,903 cm^{-1}, $^3A_{2g} \rightarrow {}^3T_{2g}$ (ν_1); 15,748 cm^{-1}, $^3A_{2g} \rightarrow {}^3T_{1g}$ (F) (ν_2); 19,048 cm^{-1}, $^3A_{2g} \rightarrow {}^3T_{1g}$ (P) (ν_3), indicating octahedral geometry of the Ni complex [44, 45]. The band at 23,529 cm^{-1} refers to LMCT [41].

The reflectance spectrum of **4** shows a broad band at 15,600–17,513 cm^{-1} where three transitions, $^2A_1 \rightarrow {}^2A_2$, $^2A_1 \rightarrow {}^2B_1$ and $^2A_1 \rightarrow {}^2B_2$, are expected of the $3d^9$ copper(II) ion. There is a tendency that tetrahedral complexes show distortion from tetrahedral to square planar [46a]. A shoulder at 27,473 cm^{-1} can be due to the LMCT [46b].

3.5. *Thermogravimetric studies*

The thermoanalytical results of the complexes are illustrated in table 4. Decomposition of **1** occurs in three successive decomposition steps within the range 30–750°C. First, water was released in an endothermic step within the range 30–140°C. The second and third steps within the range 140–750°C can be assigned to the removal of 2HCl along with the decomposition of the ligands with a final oxide residue of $1/2Fe_2O_3$; this degradation is accompanied by an exothermic peak.

The TG curve of **3** showed that decomposition occurred in three closed steps within the temperature range 40–500°C. The first step in the range 40–150° is liberation of hydrated water with an endothermic effect. The second decomposition step at

Table 4. Thermal analysis data for **1**, **3**, **4**, **6** and **7**.

Complex	TG range (°C)	DTG (°C)	*n**	Found (Calculated)%		Assignment	Metallic residue
				Mass loss	Total mass loss		
1	30–140	65	1	6.24 (6.12)		Loss of $2H_2O$	½ Fe_2O_3
	140–750	275, 410	2	81.00 (80.31)	87.24 (86.43)	Loss of 2HCl, H_2ten and ala	
3	40–150	110	1	9.75 (9.13)		Loss of $3H_2O$	NiO
	150–310	270	1	43.31 (43.39)		Loss of HCl, H_2O and partial decomposition of H_2ten	
	310–500	405	1	35.25 (34.86)	88.31 (87.38)	Loss of remaining H_2ten and ala	
4	100–320	230	1	11.12 (10.96)		Loss of CO_2, CH_4	CuO
	320–700	340, 470	2	74.80 (74.53)	85.92 (85.49)	Loss of ala and H_2ten	
6	100–250	200	1	2.4 (2.65)		Loss of coordinated water	UO_2
	250–780	285,555	2	57.50 (57.63)	62.90 (62.28)	Decomposition of Hten and ala	
7	100–300	230	1	1.65 (1.94)		Loss of coordinated water	UO_2
	300–750	470, 550	1	68.90 (68.99)	70.55 (70.93)	Decomposition of the Hten ligand	

*n = Number of decomposition steps.

150–310°C corresponds to loss of HCl, coordinated water and partial decomposition of H_2ten accompanied with successive endo- and exothermic peaks. The third remaining decomposition step is from 310–500°C corresponding to loss of remaining ligands leaving NiO residue with activation energy of 178.6 kJ mol^{-1}. DTA shows two exothermic signals.

[Cu(H_2ten)(ala)]AcO thermally decomposed in two indefinite successive decomposition steps with total estimated mass loss of 85.92% within the temperature range 100–700°C, attributed to liberation of CO_2 and CH_4 followed by loss of ligands in the second step leaving residual CuO (total calculated mass loss = 85.49%). These two steps are accompanied by two endothermic DTA signals.

[UO_2(Hten)(ala)(H_2O)] thermally decomposed in three successive decomposition steps. The first step within the range 100–250°C may be attributed to liberation of the coordinated water with an endothermic effect. The second and third decomposition steps occurred within the range 250–780°C from decomposition of both ligand molecules leaving UO_2 as a residue. This decomposition had successive endo- and exothermic signals.

The TG curve of **7** showed that the decomposition occurred in two steps. The first step within the range 100–300°C corresponds to loss of water; the DTA exhibited an endothermic peak. The second step within the range 300–750°C corresponds to the complete decomposition of the ligand and formation of UO_2 as a final pyrolysis product. This process is connected with successive endothermic and exothermic effects.

3.6. *Kinetic studies*

The kinetic and thermodynamic parameters such as activation energy (ΔE^*), enthalpy (ΔH^*), entropy (ΔS^*) and free energy change of the decomposition (ΔG^*) were evaluated graphically by employing the Coats–Redfern relation [48]:

$$\log\left[\log\frac{\{W_f/W_f - W\}}{T^2}\right] = \log\left[\frac{AR}{\theta E^*}\left(\frac{1-2RT}{E^*}\right)\right] - \frac{E^*}{2.303\ RT} \quad (1)$$

where W_f is the mass loss at the completion of the reaction, W is the mass loss up to temperature T, R is the gas constant, E^* the activation energy in kJ moL^{-1}, θ is the heating rate and $(1-(2RT/E^*)) \cong 1$. A plot of the left-hand side of Eqn. (1) against $1/T$ gives a slope from which E^* was calculated and A (Arrhenius constant) was determined from the intercept. The activation entropy ΔS^*, the activation enthalpy ΔH^* and the free energy of activation ΔG^* were calculated from standard equations. The calculated values of E^*, A, ΔS^*, ΔH^* and ΔG^* for the decomposition steps are given in table 5. The most significant result is the considerable thermal stability of the complexes reflected from the high values of the activation energy for decomposition. The second essential result from table 5 is that the entropy change ΔS^* for the formation of the activated complexes from the starting reactants has negative values in all the cases. This negative sign suggests that the degree of structural arrangement or organization of the activated complexes was lower than that of the starting reactants and the decomposition reactions are slow reactions [48].

Table 5. Kientic and thermodynamic data of the thermal decomposition for **1**, **3**, **4**, **6** and **7**.

Complex	Decomposition range (°C)	E^* (kJ moL^{-1})	A (s^{-1})	ΔS^* (JK^{-1} moL^{-1})	ΔH^* (kJ moL^{-1})	ΔG^* (kJ moL^{-1})
1	30–140	58.19	3.04×10^{10}	−43.96	39.78	84.09
	140–750	206.2	6.96×10^{7}	−108.4	175.6	190.7
3	40–150	41.08	4.78×10^{6}	−52.37	56.76	47.78
	150–310	113.6	1.75×10^{12}	−96.06	129.4	95.37
	310–500	178.6	6.07×10^{10}	−122.5	153.4	142.5
4	100–320	54.23	2.24×10^{8}	−75.22	85.66	57.63
	320–700	114.6	3.05×10^{11}	−132.8	175.3	112.9
6	100–250	36.85	6.05×10^{10}	−32.98	47.17	56.65
	250–480	97.85	2.19×10^{13}	−85.77	83.78	103.2
	480–780	167.7	4.59×10^{8}	−135.9	146.7	175.4
7	100–300	30.61	3.13×10^{8}	−55.16	36.57	46.96
	300–750	148.3	5.75×10^{10}	−92.72	99.83	134.5

3.7. *Structural interpretation*

On the basis of the structural information from elemental analysis, IR, Raman, molar conductance and thermal analysis, we propose that **1**, **2** and **3** are octahedral complexes, while **4** and **5** are tetrahedral complexes; furthermore, **6** and **7** are pentagonal bipyramidal complexes. Ternary complexes exhibit a (N, O) coordination mode (N=N1′) of the pyridine group of H_2ten or amino group of Hala; (O=O15) from the amide group of H_2ten or carboxylate group in Hala. Thus, H_2ten is a neutral bidentate ligand coordinated to the metal ions via the pyridine-N and carbonyl-O groups, while Hala is a uninegative bidentate ligand coordinated to the metal ions via amino-N and deprotonated carboxylate-O groups. The proposed geometrical structures are given in figure 2.

3.8. *NMR spectroscopy*

In order to study the dissociated species that exist in DMSO solution ^{1}H and ^{13}C NMR spectra of **5** were recorded. The signal assignments are presented in table 6. The spectra of **5** resemble the spectra of the corresponding H_2ten and Hala ligands. Only small differences in chemical shifts are found. Upon standing for a few minutes, the DMSO solution of **5** becomes cloudy, which is attributed to precipitation of **9**, therefore ^{1}H and ^{13}C NMR display several additional peaks, revealing the presence of the free amino acid in equilibrium with other complex species. All signals in the complex are shifted to higher fields relative to H_2ten. The difference in chemical shift between the peaks for H_2ten and Zn(II) chelate are related to the coordination of the pyridine nitrogen N1′ of tenoxicam which modifies the electronic environment around the vicinal protons (figure 1). The shift in the aromatic protons may be due to the donation of electron density of Zn upon chelation. The signal of the proton attached to N16 is shifted to higher field, consistent with formation of an intramolecular hydrogen bond with the keto group O17. A downfield shift is observed for CH and methyl groups of dl-alanine on comparison with the spectra of the free amino acid; this may be due to formation of hydrogen bonding to the sulfoxide oxygen. A large upfield shift, as expected for the CO carbon, can be due to coordination of carboxylate oxygen to zinc.

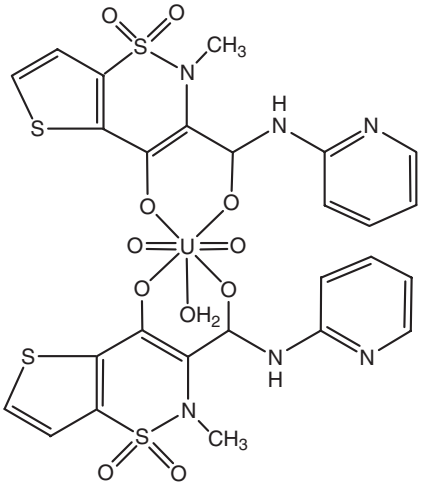

UO_2(VI) binary chelate

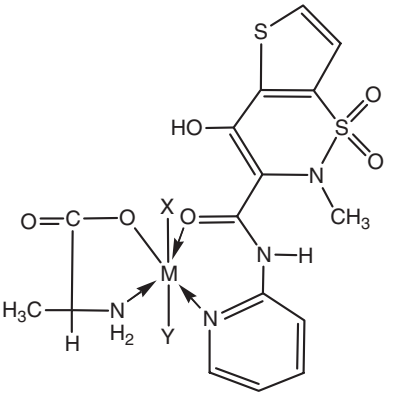

1: M = Fe(III), X = Y = Cl, n = 2
2: M = Co(II), X = Cl, Y = H_2O, n = 2
3: M = Ni(II), X = Cl, Y = H_2O, n = 3

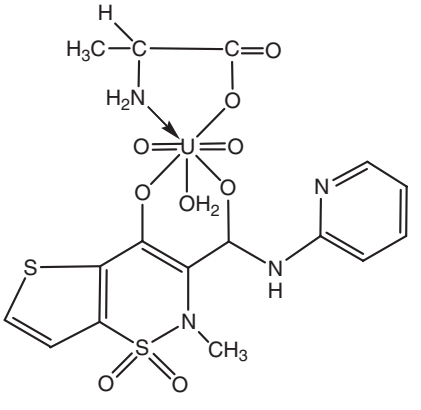

UO_2(VI) ternary chelate

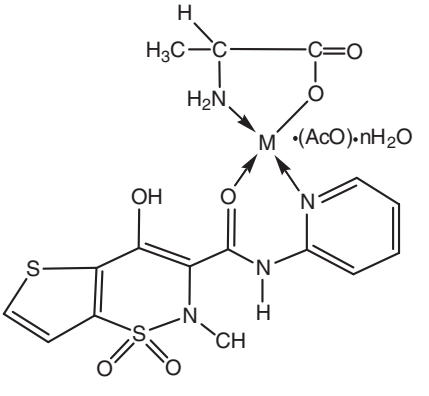

M = Cu(II), (n = 0); Zn(II) (n = 3).

Figure 2. Proposed chemical structures of the metal chelates.

3.9. *X-ray structure of* trans,trans-*[Co(II)(Hten)$_2$(dmso)$_2$] (8) and* trans,trans-*[Zn(II)(Hten)$_2$(dmso)$_2$] (9)*

Representative structural views of **8** and **9** with the selected atom numbering is shown in figures 3 and 4, respectively. Selected bond distances and angles are summarized in table 7.

Complex **8** is isostructural with complex **9**. Both crystallize in the monoclinic system with space group $P2_1/n$. The metal center has a pseudo-octahedral coordination arrangement with the metal located on an inversion center. The $Hten^-$ anions chelate the metal center through the nitrogen atoms from pyridine N3 and through the amidic oxygen O4 at the equatorial positions (with a *trans* arrangement). The apical (axial) coordination sites are occupied by O5 of the two dmso ligands. The Co–N3 and Zn–N3

Table 6. ^{1}H and ^{13}C NMR chemical shifts of tenoxicam ligand and $[Zn(H_2ten)(ala_2)](AcO)\cdot 3H_2O$ (**5**) complex in DMSO-d_6. δ in ppm.

		H_2ten		(**5**)	
^{1}H	^{13}C	^{1}H	^{13}C	^{1}H	^{13}C
H(3′)	C(2′)	8.26,8.23(d)	154.0	7.91, 8.03(d)	153.26
H(4′)	C(3′)	7.79,7.74(m)	116.0	7.67, 7.69(m)	115.04
H(5′)	C(4′)	7.15,7.13(t)	140.0	7.36, 7.43(t)	140.5
H(6′)	C(5′)	8.38,8.36(d)	120.0	8.316(br)	118.31
H(6)	C(6′)	8.03(d)	145.0	7.85(d)	146.85
H(7)	C(3)	7.46(d)	110.2	7.098(br)	107.91
H (CH_3)	C(4)	2.96(s)	160.8	0.85(s)	159.57
H(N16)	C(6)	8.76(s, br)	125.0	4.313(s,br)	122.98
H(O17)	C(7)	13.25(s, br)	126.8		124.85
	C(13)		41.0		41.5
H(CH, Hala)	C(14)		167.0	3.31(br)	166.31
H(CH_3, Hala)	C(8)		134	1.06(d)	131.2
H(NH_2, Hala)				3.44(br)	
H(OH, Hala)	C(9)		129	13.36(s, br)	124.0
	C(CH_3, Hala)				18.8(br)
	C(CH, Hala)				56.35
	C(CO, Hala)				170.3
H(CH_3, AcO)	C(CH_3, AcO)			2.87(s)	19.2(br)
H(OH, AcO)				13.93(s, br)	

[a] δ (TMS) = 0.0 ppm; C-atoms are numbered according to the numbering scheme of the carbon atoms in figure 1.

bond lengths are 2.156(1) and 2.154(1) Å, respectively, slightly longer than the values found for similar complexes [*trans*,*trans*-[Co(II)(Hmel)$_2$(dmso)$_2$] and [Zn(II)(Hmel)$_2$(dmso)$_2$] [Hmel$^-$, monoanionic of meloxicam] [49], while the bond lengths of Co–O4 (2.031(1) Å) and Zn–O4 (2.032(1) Å) are shorter than values found for those complexes.

3.9.1. The Hten$^-$ ligand. The tenoxicam ligand is deprotonated at O17 and adopts the 17,1′-ZZZ conformation around C(3)–C(14), C(14)–N(16), N(16)–C(2′) linkages (see figure 1, above). The chelating anion is stabilized by a strong intramolecular hydrogen bond which involves the O3 and N2 atoms (O···N, 2.61(1) and 2.608(1) Å; O···H–N, 143.4(17) and 145.8(17)°) for **8** and **9**, respectively. The C5-C6 bond distances are 1.410(1) and 1.406(2) Å for **8** and **9**, respectively, slightly longer than the corresponding value for metal-free and fully protonated H_2mel (1.363(3) Å) [49] and similar to the values found for *trans*,*trans*-[Cd(II)(HPir)$_2$(dmf)$_2$] [21], *trans*,*trans*-[Cd(II)(Hten)$_2$(dmso)$_2$] [18] and *trans*,*trans*-[M(II)(Hmel)$_2$(dmso)$_2$] (M=Co(II), Cd(II) and Zn(II)) [49]. In contrast the O3–C5 bond lengths are 1.273(1) and 1.271(1) Å for **8** and **9**, respectively, shorter than the value found for H_2mel (1.336(2) Å) [49] and similar to values found for *trans*,*trans*-[Cd(II)(HPir)$_2$(dmf)$_2$] [21], *trans*,*trans*-[Cd(II)(Hten)$_2$(dmso)$_2$] [18] and *trans*,*trans*-[M(II)(Hmel)$_2$(dmso)$_2$] (M=Co(II), Cd(II) and Zn(II)) [49]. This can be explained through deprotonation at O3 and is in agreement with a significant Π conjugation in the O3/N3 system. The torsion angles C7–C6–C5–O3 [−3.8(1)° and −3.7(2)°], C5–C6–C7–N2 [−2.30(1)° and −2.50(2)°] and C5–C6–C7–O4 [179.5(3)° and 179.7(1)°] for **8** and **9**, respectively, indicate the planarity of the O3–C5–C6–C7(O4)–N2 system.

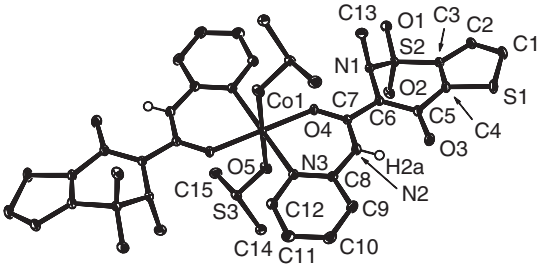

Figure 3. ORTEP drawing of trans,trans-[Co(II)(Hten)$_2$(dmso)$_2$] (**8**), with atom labels. Ellipsoids enclose 50% probability. Most hydrogen atoms omitted for clarity.

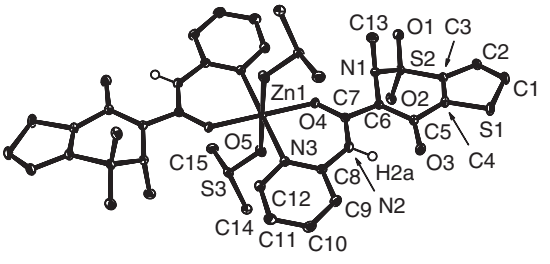

Figure 4. ORTEP drawing of trans,trans-[Zn(II)(Hten)$_2$(dmso)$_2$] (**9**), with atom labels. Ellipsoids enclose 50% probability. Most hydrogen atoms omitted for clarity.

The S2–O1 and S2–O2 bond lengths are 1.433(1) Å and 1.433(1) Å; 1.435(1) and 1.434(1) Å for **8** and **9**, respectively, and are close to the values for [Cd(II)(HPir)$_2$(dmf)$_2$] [21], *trans*,*trans*-[Cd(II)(Hten)$_2$(dmso)$_2$] [18] and *trans*,*trans*-[M(II)(Hmel)$_2$(dmso)$_2$] [M=Co(II), Cd(II) and Zn(II)] [49]. The S2-N1 bond length is 1.636(1) Å and 1.635(1) Å for **7** and **8**, respectively. These values are very close to the value reported for *trans*,*trans*-[Cd(II)(Hten)$_2$(dmso)$_2$] [18] and with those found for other C–SO$_2$–NH–C groups [50].

3.9.2. Dmso ligand. The ambidentate dmso ligand has two possible donor coordination sites, O5 and S3, the first donor site being preferred for **8** and **9**. This can be explained on the basis of steric hindrance and the relatively hard character of the cations used [Co(II) and Zn(II)]. The O5–S3 bond lengths have the same value in both complexes [1.526(1) Å] and are similar to those found for *trans*,*trans*-[Cd(II)(Hten)$_2$(dmso)$_2$] [18] and *trans*,*trans*-[M(II)(Hmel)$_2$(dmso)$_2$] [M=Co(II), Cd(II) and Zn(II)] [49]. The O5–S3–C14 and O5–S3–C15 bond angles are 104.78(4)° and 108.83(5)°; 104.82(4)° and 140.33(6)° for **8** and **9**, respectively.

3.10. *X-ray structure of* cis,cis-*[UO$_2$(VI)(Hten)$_2$(H$_2$O)]·2C$_2$H$_5$OH (7a)*

The crystal structure of **7a** is somewhat different from **8** and **9** in that it contains two crystallographically independent molecules of tenoxicam in the asymmetric unit (figure 5). Selected bond distances and angles are listed in table 7. It crystallizes in the

Table 7. Selected bond lengths (Å) and angles (deg) of *cis,cis*-$[UO_2(VI)(Hten)_2(H_2O)] \cdot 2C_2H_5OH$ (**7a**), *trans,trans*-$[Co(II)(Hten)_2(dmso)_2]$ (**8**) and *trans,trans*-$[Zn(II)(Hten)_2(dmso)_2]$ (**9**).

Co1–O4	2.031(1)	Zn1–O5	2.141(1)
Zn1–O4	2.032(1)	C19–C21	1.441(3)
U1–O1	1.773(2)	C19–N4	1.450(3)
U1–O5	2.416(2)	C22–N5	1.397(3)
U1–O4	2.323(2)	N6–C22	1.337(3)
U1–O9	2.402(2)	N3–C9	1.353(3)
U1–O8	2.325(2)	C8–C6	1.483(3)
Co1–N3	2.156(1)	S2–O7	1.429(2)
Zn1–N3	2.154(1)	S2–O6	1.426(2)
U1–O3	1.782(2)	C6–C5	1.410(1)
Co1–O5	2.118(1)	C6–C7	1.438(1)
O4–Co1–N3	93.45(2)	C21–O9–U1	136.2(1)
O4–Zn1–N3	87.11(3)	C17–C18–O8	117.1(2)
O4–Co1–O5	88.21(2)	C4–C5–O4	117.0(2)
O4–Zn1–O5	87.86(3)	C8–N3–Co1	125.9(1)
O1–U1–O3	177.6(1)	C8–N3–Zn1	125.2(1)
O5–U1–O4	70.06(6)	C5–O4–U1	138.0(1)
O9–U1–O8	70.38(6)	C18–O8–U1	137.5(2)
N3–Co1–O5	86.15(3)	C6–N1–C7	113.3(2)
N3–Zn1–O5	93.19(4)	C19–N4–C20	113.7(2)
O6–S2–O7	119.1(2)	C7–N1–S2	114.2(2)
O10–S4–O11	118.9(1)	C20–N4–S4	114.7(2)
O6–S2–N1	107.9(1)	C9–N2–C8	129.8(2)
O11–S4–N4	108.3(1)	C22–N5–C21	129.5(2)
O7–S2–N1	108.0(1)	O5–C8–N2	120.3(2)
C7–O4–Co1	131.4(1)	O9–C21–N5	120.2(2)
C7–O4–Zn1	131.0(1)	C9–N2–C8	129.8(2)
C8–O5–U1	136.5(2)	C22–N5–C21	129.5(2)

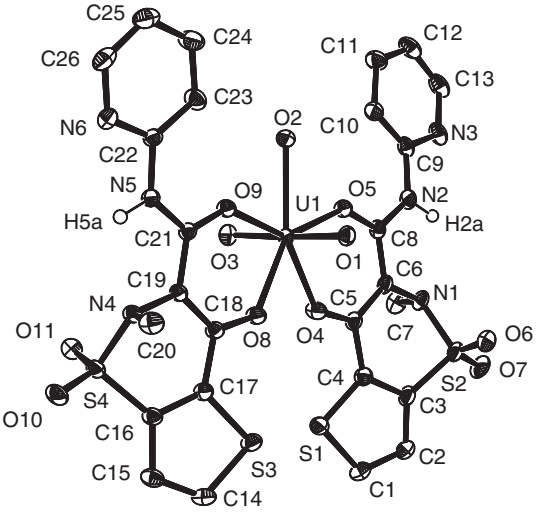

Figure 5. ORTEP view of *cis,cis*-$[UO_2(VI)(Hten)_2(H_2O)] \cdot 2C_2H_5OH$ (**7a**) with atom labels. Ellipsoids enclose 50% probability. The ethanol molecules have been omitted for clarity.

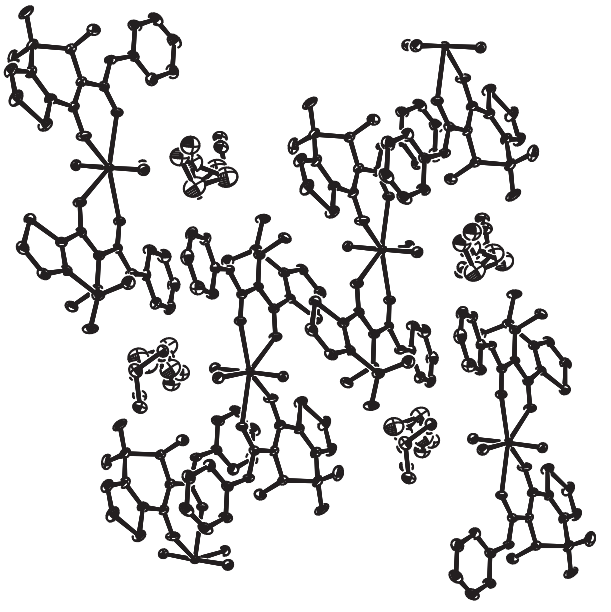

Figure 6. ORTEP view of crystal structure for *cis,cis*-$[UO_2(VI)(Hten)_2(H_2O)] \cdot 2C_2H_5OH$ (**7a**) showing the channels occupied by ethanol molecules.

triclinic space group $P\bar{1}$. The uranium is hepta-coordinate through enolate oxygen atom and the carbonyl oxygen atom of amide group of two tenoxicam molecules and one water molecule. Mohamed *et al.* [51] published UO_2^{2+}-complexes of piroxicam where the uranium ions exhibited octahedral coordination spheres and were coordinated through pyridyl nitrogen and carbonyl oxygen of the amide group.

The uranyl group is nearly linear with an O1–U–O3 angle of 177.58(8)° and normal U–O distance [d(U1–O1) = 1.773(2) Å, d(U1–O3) = 1.782(2) Å] [52]. The equatorial U–O distances separate into three groups, 2.398(2) Å for O2, average 2.324(2) Å for O4 and O8, and average 2.410(2) Å for O9 and O5. The adjacent equatorial O-U-O angles range from 70.06(6) to 73.39(6)°.

The tenoxicam ligand adopts EZE conformation (figure 1) where the chelating anion is stabilized by four hydrogen bonds (two from each side), two intramolecular hydrogen bonds between the amide nitrogen and the neighboring nitrogen from the other side N1 and N5 (N2–H2A···N1 = 2.680(1) Å; ∠=111.4(2)°) (N5–H5A···N4 = 2.681(3) Å; ∠= 111.6(1)°). Additionally, the pyridyl nitrogen is involved in two intermolecular hydrogen bonds with the oxygen of ethanol. The interatomic distances and angles of these intermolecular hydrogen bonds are not further discussed due to the disorder of the ethanol molecules.

The S2–O6, S2–O7, S4–O10 and S4–O11 bond lengths are all in the range of 1.430(1) Å, close to the values observed in **8** and **9**. The S2–N1 and S2–N4 bond lengths are 1.660(1) and 1.650(1) Å, respectively, which are similar to the values reported in **8** and **9**.

All atoms of the ethanols are heavily disordered over two positions, occupying channels running through the lattice (figure 6). A remarkable feature of the solvate crystal structure is the way in which the ethanol molecules pack (head-to-tail) into parallel channels in the lattice along the a-axis. From these data it can be seen that

uranium is heptacoordinate, with a linear uranyl ion coordinated to two bidentate tenoxicam ligands and one water molecule.

4. Conclusion

This work describes the synthesis and structural characterization of uranyl and transition metal complexes with tenoxicam (H_2ten) and dl-alanine (Hala). The complexes are obtained in high yield through simple reaction of the relevant metal acetate, chloride and nitrate and the drug with the amino acid in ethanol. All chelates show coordination behavior reported for other piroxicam and tenoxicam metal chelates. Tenoxicam is a neutral bidentate chelating ligand through the pyridyl nitrogen and the amide oxygen and adopts ZZZ conformations in **1**, **2**, **3**, **4**, **5**, **8** and **9**, while in **6**, **7** and **7a** it acts as a monoanionic ligand through enolate oxygen and amide oxygen and adopts EZE conformations. Alanine is a uninegative bidentate ligand coordinated to the metal ions via the deprotonated carboxylate-O and amino-*N*. *trans*,*trans*-[Co(II)(Hten)$_2$(dmso)$_2$] (**8**) and *trans*, *trans*-[Zn(II)(Hten)$_2$(dmso)$_2$] (**9**) complexes have no unusual intermolecular contacts in the unit cell and have no co-crystallized water molecules, although crystal growth was carried out in air. This confirms the hydrophobic character of the complex which is important for pharmacological properties. The hydrophobicity of the metal based pharmaceuticals is favored to prevent decomposition in biological buffer solutions and to facilitate their transportation through cell membranes [53]; in addition, formation of stable chelates protects the drug molecules from enzymatic degradation.

These complexes may exchange ligands, thus, the binary complexes **8** and **9** were obtained from DMSO-solutions of **2** and **5** as single crystals.

For *cis*,*cis*-[UO_2(VI)(Hten)$_2$(H_2O)] · 2C_2H_5OH (**7a**), intra- and intermolecular hydrogen bond interactions are observed which stabilize the crystal structure. The ethanol molecules are disordered in two positions and are not coordinated to the uranium but occupy parallel channels running through the lattice.

According to the kinetic data, all the complexes have negative entropy values, which indicate the complexes have more ordered systems than reactants and that the decomposition reactions are slow.

This work was undertaken to shed more light on the chelation behavior of tenoxicam in the presence of another ligand, dl-alanine, in solid state, to help in understanding the mode of chelation of each ligand towards the metal ions and the conformational space and electronic properties of such ligands.

Supplementary data

Crystallographic data (excluding structure factors) for the structures reported in this paper have been deposited with the Cambridge Crystallographic Centre as supplementary publication No. CCDC 626495 (**7a**), CCDC 626496 (**8**) and CCDC 626497 (**9**). Copies of the data can be obtained free of charge on application to CCDC,

12 Union Road, Cambridge CB2 IEZ, UK (Fax: + 44-1223/336-033; Email: deposit@ ccdc.cam.ac.uk).

Acknowledgements

The authors are thankful to J. Wagler for his help and useful discussion. N.E.A. El-Gamel is grateful to the Alexander von Humboldt Foundation, Bonn, Germany for financing a 9 month stay at the Inorganic Institute, TU Bergakademie Freiberg, Germany.

References

[1] (a) C. Orvig, M. Abrams. *J. Chem. Rev*., **99**, 2201 (1999); (b) K.H. Thompson, J.H. McNeill, C. Orvig. *Chem. Rev*., **99**, 2561 (1999); (c) H. Sun, H. Li, P. Sadler. *J. Chem. Rev*., **99**, 2817 (1999); (d) N.P. Farrell. *Uses of Inorganic Chemistry in Medicine*, Royal Society of Chemistry, Cambridge, UK (1999), Ch. 3 and references therein; (e) R. Cini. *Comments Inorg. Chem*., **22**, 151 (2000).
[2] E.J. Baran. *Quim. Bioinorg*., McGraw-Hill Interamericana, Madrid (1995).
[3] P. Emery, S.X. Kong, E.W. Ehrich, D.J. Watson, T.E. Towheed. *Clin. Therapeut*., **24**, 1225 (2002).
[4] (a) J.E. Weder, C.T. Dillon, T.W. Hambley, B.J. Kennedy, P.A. Lay, J.R. Biffin, H.L. Regtop, N.M. Davies. *Coord. Chem. Rev*., **232**, 95 (2002); (b) J.P. Gonzalez, P.A. Todd. *Drugs*, **34**, 289 (1987).
[5] E.H. Wiseman, J.G. Lombardino. *Eur. J. Rheumatol. Inflamm*., **4**, 280 (1981).
[6] S.K. Hadjikakou, M.A. Demertzis, J.R. Miller, D. Kovala-Demertzi. *J. Chem. Soc., Dalton Trans*., 663 (1999).
[7] (a) R. Cini, G. Giorgi, A. Cinquantini, C. Rossi, M. Sabat. *Inorg. Chem*., **29**, 5197 (1990); (b) R. Cini. *J. Chem. Soc., Dalton Trans*., 111 (1996); (c) D. Di Leo, F. Berrettini, R. Cini. *J. Chem. Soc., Dalton Trans*., 1993 (1998).
[8] M.R. Caira, L.R. Nassimbeni, M. Timme. *J. Pharm. Sci*., **84**, 884 (1995).
[9] E. Bernhard, F. Zimmermann. *Arzneim.-Forsch*., **34**, 647 (1984).
[10] R.-S. Tsai, P.-A. Carrupt, N. El-Tayar, Y. Giroud, P. Adrade, B. Testa, F. Breé, J.-P. Tillement. *Helv. Chim. Acta*, **76**, 842 (1993).
[11] M.R. Moya-Hernández, A. Mederos, S. Domínguez, A. Orlandini, C.A. Ghilardi, F. Cecconi, E. González-Vergara, A. Rojas-Hernández. *J. Inorg. Biochem*., **95**, 131 (2003).
[12] O. Atay, F. Dincol. *Anal. Lett*., **30**, 1675 (1997).
[13] A.F.M. ElWalily, S.M. Blaih, M.H. Barary, M.A. ElSayed, H.H. Abdine, A.M. ElKersh. *J. Pharmaceut. Biomed. Anal*., **15**, 1923 (1997).
[14] Z. Atkopar, M. Tuncel. *Anal. Lett*., **29**, 2383 (1996).
[15] M.S. Garcia, C. Sanchez-Pedreno, M.I. Albero, M.J. Gimenez. *J. Pharm. Biomed. Anal*., **21**, 731 (1999).
[16] D.W. Blake, A.R. Bjorksten, F.C. Libreri. *Anaesthesia and Intensive Care*, **25**, 142 (1997).
[17] A. Bury, A.E. Underhil, D.R. Kemp, N.J. O'Shea, J.P. Smith, P.S. Gomm. *Inorg. Chim. Acta*, **138**, 85 (1987).
[18] S. Defazio, R. Cini. *Polyhedron*, **22**, 1355 (2003).
[19] N. Abo El-Maali, J.C. Vire, G.J. Patriarche, M.A. Ghandour. *Anal. Lett*., **2**, 3025 (1989).
[20] H.A. Mohamed, H.M.A. Wadood, O.A. Farghaly. *J. Pharm. Biomed. Anal*., **28**, 819 (2002).
[21] (a) D. Kovala-Demertzi. *J. Organomet. Chem*., **691**, 1767 (2006); (b) M.A. Demertzis, S.K. Hadjikakou, D. Kovala-Demertzi, A. Koutsodimou, M. Kubicki. *Helv. Chim. Acta*, **83**, 2787 (2000); (c) S.K. Hadjikakou, M.A. Demertzis, J.R. Miller, D. Kovala-Demertzi. *J. Chem. Soc., Dalton Trans*., 663 (1999).
[22] For Zn(II), (a) J.W.L. Nascimento, L.H. Santos, M.S. Nothenberg, M.M. Coelho, S. Oga, C.A. Tagliati. *Pharmacology*, **68**, 64 (2003); (b) J.W.L. Nascimento, C.A. Tagliati, M.S. Nothenberg, S. Oga, L.H. Santos. *Braz. Pedido Pl* (2001), BPXXDX BR 2099003666 A 20010522, Portuguese Patent. For Cu(II), J.R. Sorenson. *J. Med. Chem*., **19**, 135 (1976); (b) J.R. Sorenson. *Prog. Med. Chem*., **26**, 437 (1989).
[23] (a) E. Larrucea, A. Arellano, S. Santoyo, P. Ygartua. *Drug Development and Industrial Pharmacy*, **28**, 245 (2002); (b) E. Larrucea, A. Arellano, S. Santoyo, P. Ygartua. *Drug Development and Industrial Pharmacy*, **27**, 251 (2001); (c) Ju-H. Kim, H-K. Choi. *Yakche Hakhoechi*, **30**, 33 (2000); (d) Z. Aigner, A. Kezmarki, M. Kata, C. Novak, I. Eroes. *J. Inclusion Phenom. Macrocyclic Chem*., **42**, 227 (2002).

[24] (a) M.A. Zayed, F.A. Nour El-Dien, G.G. Mohamed, N.E.A. El-Gamel. *Spectrochim. Acta*, **64A**, 216 (2006); (b) M.A. Zayed, F.A. Nour El-Dien, G.G. Mohamed, N.E.A. El-Gamel. *Spectrochim. Acta*, **60A**, 2843 (2004).
[25] S. El-Khateeb, S. Abdel Fattah, S. Abdel Razeg, M. Tawakkol. *Anal. Lett.*, **22**, 101 (1989).
[26] E. Santi, M.H. Torre, E. Kremer, S.B. Etcheverry, E.J. Baran. *Vib. Spectrosc.*, **5**, 285 (1993).
[27] W. Radecka-Paryzek, E. Luks. *Monatsh. Chem.*, **126**, 795 (1995).
[28] J. Costamagna, F. Carruso, M. Rossi, M. Campos, J. Canales, J. Ramirez. *J. Coord. Chem.*, **54**, 247 (2001).
[29] (a) G.G. Mohamed, N.E.A. El-Gamel. *Spectrochim. Acta*, **60A**, 3141 (2004); (b) G.G. Mohamed, N.E.A. El-Gamel. *Vib. Spectrosc.*, **36**, 97 (2004).
[30] D.X. West, J.K. Swearingen, J. Valdes-Martinez, S. Hernandez-Ortega, A.K. El-Sawaf, F. Van Meurs, A. Castineiras, I. Garcia, E. Bermejo. *Polyhedron*, **18**, 2919 (1999).
[31] (a) K. Nakamoto, Y. Morimoto, A.E. Martell. *J. Am. Chem. Soc.*, **83**, 4533 (1961); (b) G.K.T. Conn, C.K. Wu. *Trans. Faraday Soc.*, **34**, 1483 (1938); (c) H.D. Bist. *J. Mol. Spectrosc.*, **16**, 542 (1968).
[32] D.T. Haworth, G.Y. Kiel, L.M. Proniewicz, M. Das. *Inorg. Chim. Acta.*, **130**, 113 (1987).
[33] K. Nakamoto. *Infrared and Raman Spectra of Inorganic and Coordination Compounds*, 3rd Edn, Wiley, New York (1978).
[34] R.J.H. Clark, C.S. Williams. *Inorg. Chem.*, **4**, 350 (1965).
[35] R.L. Frost, K.L. Erickson, J. Cejka, B.J. Reddy. *Spectrochim. Acta*, **61A**, 2702 (2005).
[36] J.A. Dean (Ed.), *Lange's Handbook of Chemistry*, 14th Edn, Table 8.35, New York, McGraw-Hill (1992).
[37] J.J. Fiol, A. Terron, D. Mulet, V. Merno. *Inorg. Chim. Acta*, **135**, 197 (1987).
[38] Q. Zhou, T.W. Hambley, B.J. Kennedy, P.A. Lay, P. Turner, B. Warwick, J.R. Biffin, H.L. Regtop. *Inorg. Chem.*, **39**, 3742 (2000).
[39] M.T. Hay, B.J. Hainaut, S. Geib, J. Steven. *Inorg. Chem. Commun.*, **6**, 431 (2003).
[40] B.K. Santra, G.K. Lahiri. *J. Chem. Soc., Dalton Trans.*, 139 (1998).
[41] J. Manonmani, R. Thirumuruhan, M. Kandaswamy, V. Narayanan, S. Shanmuga, S. Raj, M.N. Ponnuswamy, G. Shanmugan, H.K. Fun. *Polyhedron*, **20**, 3039 (2001).
[42] M.M. Moustafa. *J. Therm. Anal.*, **50**, 463 (1997).
[43] A. Hazell, C.J. Mckenzie, L.L. Nielsen. *Polyhedron*, **19**, 1333 (2000).
[44] M. Velusamy, M. Palaniandavar, K.R.J. Thomas. *Polyhedron*, **17**, 2179 (1998).
[45] M.A. Ali, S.S.M.-H. Majumder, R.J. Butcher, J.P. Jasinski, J.M. Jasinski. *Polyhedron*, **16**, 2749 (1997).
[46] (a) P.C. Chai, D.P. Freyberg, G.M. Mockler, E. Sinn. *Inorg. Chem.*, **16**, 254 (1977); (b) K.H. Reddy, P.S. Reddy, R.P. Babu. *J. Inorg. Biochem.*, **77**, 169 (1999).
[47] A.W. Coats, J.P. Redfern. *Nature*, **201**, 68 (1964).
[48] (a) L.T. Vlaev, G.G. Gospodinov. *Thermochim. Acta*, **370**, 15 (2001); (b) A.A. Soliman, G.G. Mohamed. *Thermochim. Acta*, **421**, 151(2004); (c) A.A. Soliman, S.M. El-Medani, O.A.M. Ali. *J. Therm. Anal. Calorim.*, **83**, 385 (2006).
[49] S. Defazio, R. Cini. *J. Chem. Soc., Dalton Trans.*, **9**, 1888 (2002).
[50] F.H. Allen, O. Kennard, D.G. Watson, L. Brammer, A.G. Orpen, R. Taylor. *J. Chem. Soc., Perkin Trans. 2.*, **12**, S1 (1987).
[51] G.G. Mohamed. *Spectrochim. Acta*, **62A**, 1165 (2005).
[52] K. Umeda, J. Zulerman-Schpector, P.C. Isolani. *Polyhedron*, **25**, 2447 (2006).
[53] J.E. Weder, T.W. Hambley, B.J. Kennedy, P.A. Lay, D. MacLachlan, R. Bramley, C.D. Delfs, K.S. Murray, B. Moubaraki, B. Warwick, J.R. Biffin, H.L. Regtop. *Inorg. Chem.*, **38**, 1736 (1999).